Journal of Contaminant Hydrology 193 (2016) 21–34

Contents lists available at ScienceDirect

Journal of Contaminant Hydrology

journal homepage: www.elsevier.com/locate/jconhyd

Investigating nitrate dynamics in a fine-textured soil affected by feedlot effluents

E.A. Veizaga [a,b,*], L. Rodríguez [b], C.J. Ocampo [c]

[a] Consejo Nacional de Investigaciones Científicas y Técnicas (CONICET), Av. Rivadavia 1917, (C1033AAJ) Ciudad Autónoma de Buenos Aires, Argentina
[b] Centro de Estudios Hidroambientales (CENEHA)-Facultad de Ingeniería y Ciencias Hídricas (FICH)-Universidad Nacional del Litoral (UNL), Ciudad Universitaria. Ruta Nacional N° 168 - Km 472,4, (3000), Santa Fe, Argentina
[c] School of Civil, Environmental and Mining Engineering, University of Western Australia, 35 Stirling Highway, 6009 Crawley, Western Australia, Australia

ARTICLE INFO

Article history:
Received 8 April 2016
Received in revised form 28 June 2016
Accepted 10 August 2016
Available online 12 August 2016

Keywords:
Feedlot
Nitrate
Numerical model

ABSTRACT

Feedlots concentrate large volumes of manure and effluents that contain high concentrations of nitrate, among other constituents. If not managed properly, pen surfaces run-off and lagoons overflows may spread those effluents to surrounding land, infiltrating into the soil. Soil nitrate mobilization and distribution are of great concern due to its potential migration towards groundwater resources. This work aimed at evaluating the migration of nitrate originated on feedlots effluents in a fine-textured soil under field conditions. Soil water constituents were measured during a three-year period at three distinct locations adjacent to feedlot retention lagoons representing different degrees of exposure to water flow and manure accumulation. A simple statistical analysis was undertaken to identify patterns of observed nitrate and chloride concentrations and electrical conductivity and their differences with depth. HYDRUS-1D was used to simulate water flow and solute transport of Cl^-, NO_4^+—N, NO_3^-—N and electrical conductivity to complement field data interpretation. Results indicated that patterns of NO_3^-—N concentrations were not only notoriously different from electrical conductivity and Cl^- but also ranges and distribution with depth differed among locations.

A combination of dilution, transport, reactions such as nitrification/denitrification and vegetation water and solute uptake took place at each plots denoting the complexity of soil-solution behavior under extreme polluting conditions.

Simulations using the concept of single porosity-mobile/immobile water (SP-MIM) managed structural controls and correctly simulated $^-$all species concentrations under field data constrains. The opposite was true for the other two locations experiencing near-saturation conditions, absence of vegetation and frequent manure accumulation and runoff from feedlot lagoons.

Although the results are site specific, findings are relevant to advance the understanding of NO_3^-—N dynamics resulting from FL operations under heavy soils.

1. Introduction

Historically, beef cattle production has been one of the traditional activities and significant support to the economic growth of Argentina (Guevara and Grünwaldt, 2012). Until the 1990s, 100% of cattle were grazed in rangeland. Towards the end of the 1980s, a steady increase in soybean planting started competing for land with the meat industry. Cattle were either displaced from traditional production areas in Argentina's Pampa plains to other regions of the country or raised in confined cattle operations (feedlots-FL) (Arelovich et al., 2011). Due to flawed legislation and environmental controls, the rapid growth of FL activities has generated environmental concerns because of the potential point and diffuse source of pollution these establishments may produce.

FLs concentrate large volumes of manure by-products and effluents vulnerable to weathering if not properly managed. Manure accumulated on the surface of pens is periodically removed and temporarily placed in stockpiles. Waste retention lagoons are common systems to hold FL effluents (Pordomingo, 2003). However, wastes not promptly removed from corrals or managed within FLs are subject to environmental factors; inadequate maintenance of retention lagoons may cause unwelcome environmental consequences to soils and groundwater surrounding these structures. Pen surfaces and stockpiles-generated run-off and lagoons overflows may spread solid and liquid effluents to surrounding land (Veizaga, 2015).

* Corresponding author at: Consejo Nacional de Investigaciones Científicas y Técnicas (CONICET), Av. Rivadavia 1917, (C1033AAJ) Ciudad Autónoma de Buenos Aires, Argentina.
E-mail addresses: veizaga.e82@gmail.com, e.veizaga@conicet.gov.ar (E.A. Veizaga).

http://dx.doi.org/10.1016/j.jconhyd.2016.08.005
0169-7722/

Manure solutions resulting from surface runoff after precipitation events are composed of dissolved organic matter, nutrients, salts, antibiotics, and heavy metals, among other constituents (Sweeten, 2000; Pepple et al., 2011; García et al., 2012). Soil nitrate mobilization and redistribution in the profile are of great concern due to its potential migration towards groundwater resources.

Many pioneering studies in the 70s have focused on the characterization of soil and soil water underneath FL pen surfaces and their relation to hydrological and biogeochemical processes. These works reported little nitrate ($NO3^-$—N) mobilization below FL due to lack of infiltration (Mielke et al., 1974; Mielke and Mazurak, 1976) and high concentrations in the first 15 cm of the soil profile during the summer season that enhanced nitrification processes (Elliott et al., 1972). Lack of $NO3^-$—N presence in the subsoil was attributed to the loss of nitrate via denitrification processes.

However, more recent works have focused on the leaching and distribution of salts and nutrients deep in the soil profile and surrounding groundwater as a result of the long-term operation of FLs. Maulé and Fonstad (2000, 2002) found that 50% to 67% of sampled groundwater near five 25- to 35-year-old feedlots in central Saskatchewan (Canada) had elevated concentrations of solutes due to the presence of manure but cautioned about the use of NO_3^-—N as a reliable indicator of manure seepage due to its no-conservative nature subject to biological transformations (Maulé and Fonstad, 2002). A different pattern of the distribution of nutrient elements (nitrogen, phosphorus, potassium) and some of the elements participating in soil cation exchange have been reported below FL soils. Olson et al. (2005) found that while nutrients concentrations were significantly affected only in the top soil layer (0.15 m) of a FL in southern Alberta (Canada), remarkable increases in other soil properties were observed at a depth of 0.6 m with chloride reaching its maximum concentration at a depth of 1.5 m. Chloride accumulation in the soil profile due to leaching was also reported by other studies in the same geographical region for moderately fine and coarse soils up to a depth of 70 cm and 50 cm, respectively (Miller et al., 2008).

A growing need to investigate the chemical composition and transformation processes of waste from FL operations has driven new research. Recent studies reassessed the potential for leaching into the soil profile. Vaillant et al. (2009) observed a notable reduction in ammonium, organic nitrogen, carbon and chloride below one-meter depth in the soil profile.

Chloride (Cl^-) content in FL manure is considerably greater than in soils, and can be considered as an indicator of potential movement of nitrates due to their similarity in mobility and solubility (Tyler and Thomas, 1977). It is a stable, soluble anion not affected by biological processes. These properties make it an appropriate candidate for processes understanding and comparison with the complex dynamics of nitrate in soils below FL (Kachanoski et al., 1992; Czapar et al., 1994; Schuh et al., 1997; Lobb et al., 1999; Derby and Knighton, 2001). However, the behavior of NO_3^-—N in the unsaturated zone or groundwater varies widely from site to site. Consequently, the choice of monitoring sites becomes crucial to analyze the suitability of Cl^- as a proxy for NO_3^--N evaluation in environments that have a strong polluting activity (Baram et al., 2012a).

Flow and solute transport modeling are often used to complement field studies to gain additional insights from process-based simulations (Hanson et al., 2006; Mantovi et al., 2006; Crevoisier et al., 2008; Saso et al., 2012). Those investigations used numerical simulations to assess unsaturated flow and solute transport for Cl^- and nitrogen (N) under controlled flow and irrigation regimes, while Ramos et al. (2011) extended their research to integrate field-modeling studies for multicomponent solute transport for nitrogen. For the above studies near saturation moisture conditions of the soil profile were reached, facilitating in turn, monitoring activities, water sample collection, and numerical model result interpretations. Only more recent studies undertook field-scale experiments and modeling under real meteorological forcing within feedlot premises (Olson et al., 2005; Miller et al., 2008; Vaillant et al., 2009) and dairy farm facilities (Baram et al., 2012a, 2012b).

In the Argentine Pampas region, field investigations were recently undertaken to assess solute distribution in soils in FL pens and adjacent land affected by runoff. High concentrations of chloride at 20 cm depth were found at FL sites when compared to adjacent soils non-affected by trampling, highlighting the role of water runoff in this ambient (Wyngaard et al., 2012). These authors extended their investigation to assess whether the high concentration of these compounds, mobilized by surface runoff from FL pens, promotes movement through the soil to deeper horizons. Changes in inorganic N concentrations, urea content, urease activity in the soil up to 60 cm depth were evaluated across a topographic transect from high to low ground in an FL and adjacent pasture land. The effect of topographic location on the distribution of nitrogen species in the soil profile was profound with NH_4^+—N showing its peak between 40–60 cm depth and NO_3^-—N at a depth of 10 cm for the lower and higher topographic locations. Nonetheless, there is a lack of combined field and numerical modeling investigations to assess the fate and transport of nitrogen, and in particular NO_3^-—N—N, in an FL under natural forcing. Scarce studies on Argentina's Pampa plains soils limit the knowledge and capacity to inform suitable management strategies to mitigate negative impacts from FL operations.

The objective of the present work is to contribute towards the above issue by evaluating the transport and transformation processes of nitrate originated on FL effluents within a fine-textured soil. Several soil water constituents were measured during a three-year period at three distinct sites adjacent to effluents retention lagoons and temporary water ponding areas. The sites were carefully selected to investigate how different flows of water and manure solution accumulation on the surface affect the distribution of nitrate in the soil profile.

HYDRUS-1D was used to simulate water flow and solute transport resorting to the concept of mobile/immobile water (MIM) for solute transport of Cl^-, NH_4^+—N, NO_3^-—N concentration and electrical conductivity (EC). The analysis and interpretation of results focused on identifying: 1) the quantitative differences between plots, 2) the vertical variations, mean values, and range of the aforementioned variables; and 3) first-order controls on observed NO_3^-—N distribution in the soil profile.

2. Materials and methods

2.1. Site characteristics

The investigation was carried out in an FL establishment located 5 km north of San Justo city in the Province of Santa Fe, Argentina (30° 47′ 21″, 60° 35′ 31″) with a maximum of 9000 animal holding capacity, distributed within 33 pens that occupy 11.4 ha.

The climate in the area is temperate, with an average annual precipitation of 1057 mm (Series 1920–2011, National Institute of Agricultural Technology — INTA). Winter months (June to August) are the driest, with 40% of the annual precipitation falling in the summer months (January to March). The average minimum and maximum temperatures are 12 °C and 26 °C for the winter and summer season, respectively.

The study region is characterized by highly productive soils and an intense agricultural-livestock activity. Soil characteristics across the area correlate well with the landscape geomorphological units. At the FL and surrounding lands, soil is classified as Typic Argiudol in highland areas to Natracualf in lowland areas.

2.2. Experimental design

A detailed topographic survey performed at the feedlot premises allowed to identify the most suitable spots for water-manure solution investigation. The selected area corresponds to a topographically low zone around the effluents retention lagoons (Fig. 1). A soil pit 130 cm deep was excavated to describe soil horizons and extract disturbed

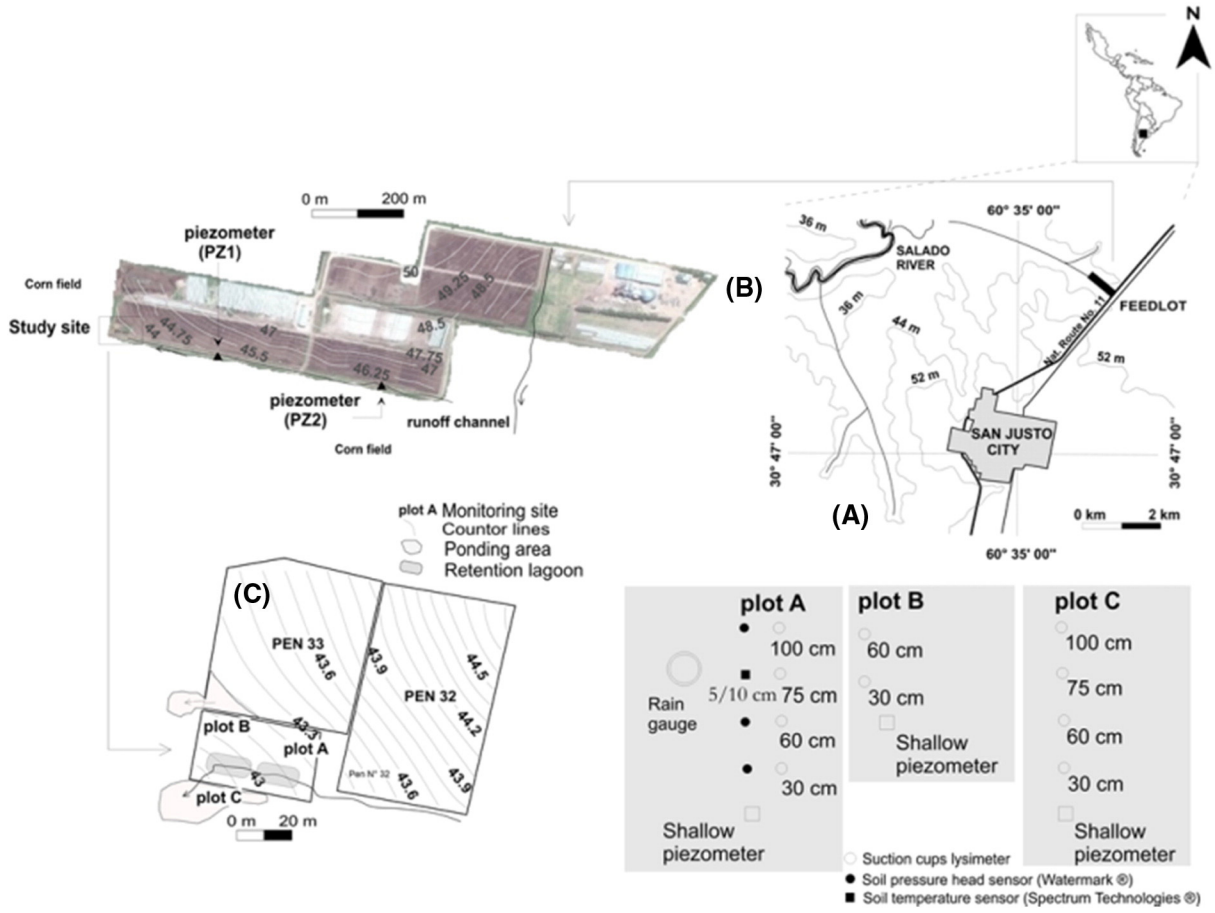

Fig. 1. (A) Location of feedlot establishment; (B) Plan view of feedlot premises indicating the study site location and contour lines- equidistance 0.25 m; (C) Schematic illustration of the field site, soil zone monitoring systems and observation wells installed: (plot A) upstream the waste lagoons, (plot B) upstream the waste lagoons near a ponding area, and (plot C) downstream the waste lagoons. Plant view of the instrumentation at each monitoring site (light-grey shaded area) and depth of the different sensors in the soil (dark-grey area) are also shown. Arrows indicate surface runoff direction.

and undisturbed soil samples with a 5 cm diameter metal cylinder. Soil horizons identification was instrumental in selecting the installation depths of different soil water characterization devices. Textural properties were determined by Bouyoucos method (Gee et al., 1986) and bulk density of each horizon by the cylinder method.

The field study comprised the instrumentation of three soil-water monitoring sites named plot A, plot B, and plot C, affected by different degrees of pollution. Fig. 1 schematically illustrates the location of the three plots and the instruments/sensors installed. Plot A, instrumented Nov-30, 2011, was located between the lagoons and a feedlot pen. This site is at a slightly higher elevation than its surroundings. Vegetation grew naturally on the soil surface during field investigations. Plot B, instrumented Feb-07, 2012, was located 35 m from plot A near a water/manure ponding area and upstream the retention lagoons. This plot was regularly affected by water-manure runoff and ponding effluents nearby that maintained near-saturation conditions for prolonged periods of time after precipitation events. Plot C, instrumented Mar-21, 2013, was located to the side of a carrying-effluents furrow formed naturally during heavy rains. This site became a directly affected place by water-manure effluents contained in the retention lagoons due to frequent overflowing.

Plot A was instrumented with Watermark ® pressure head sensors at 30, 60 and 100 cm depths linked to a Watchdog ® datalogger with a recording interval of 1 h. Soil water solution was extracted using ceramic cup lysimeters installed at the same depths. Porous ceramic cups featured an air entry pressure of 0.5/1 bar (Soilmoisture Inc. US). Only suction cups lysimeters were placed at plot B and plot C, at 30 cm and 60 cm, and at 30, 60, 75 and 100 cm depths, respectively. A shallow well (PVC-5 cm diameter) was also installed at each plot to monitor the potential for development of perched water table during the wet period. Detailed information on site description and instrumentation can be found in Veizaga et al. (2015).

Precipitation amount and intensity were measured at the site with an ODYSSEY ® datalogger hooked to a tipping bucket rain gauge. Other meteorological variables such as air temperature, relative humidity, atmospheric pressure, evaporation, wind speed, and direction were obtained from a weather station located 5 km south of the study site (operated by Ministry of Water, Public Services and Environment of Santa Fe Province). Meteorological data was used by the numerical model to compute reference evapotranspiration-Eto (Allen et al., 1998).

2.3. Monitoring approach

Fieldwork was conducted during 28 months from November 2011 to March 2014. A total of 160 soil solution samples were extracted with the lysimeters during and after precipitation events. Lysimeters were activated with a manual vacuum pump 24 h before water extraction operations. Water samples were collected with a syringe and analyzed in situ with a multiparameter probe (90MLV-TPS ®) to determine electrical conductivity EC [$\mu S\ cm^{-1}$], temperature (T) [°C] and total dissolved solids (TDS) [$mg\ cm^{-3}$]. Water samples were preserved in agreement with standards, transported and analyzed in the laboratory for Cl^- concentration (titrimetric method 4500-B) and NO_3^-—N concentration (spectroscopy UV-Vis equip BIO-TRAZA model 752 under 4500NO3-B technique, Clesceri et al., 1998). More details on soil water sampling analyzes can be found in Veizaga (2015).

2.4. Modeling approach

Numerical modeling was used to complement field results interpretation and to gain insight on process-based simulation of solute transport. HYDRUS-1D (Šimůnek et al., 2005), a standard numerical model for simulating water, heat, and solute movement in one-dimensional, variably saturated porous media, was used to simulate EC, Cl^-, NH_4^+—N and NO_3^--N distributions along the soil profile at plots A, B and C. Although other versions of HYDRUS can accommodate two-dimensional and three-dimensional flow and transport processes (Šimůnek et al., 2016), the 1D version was selected to simplify the approach and focus on differences between sites.

In single porosity media, HYDRUS-1D numerically solves Richards' equation (Richards, 1931) with finite elements techniques and selected soil hydraulic properties models, and the solute transport problem by solving the advection-dispersion equation. Notwithstanding, the presence of aggregates or cracks may affect solutes movement; their effect might be particularly pronounced in soils with high clay content causing, in turn, deviations from single-porosity solute transport models (Jarvis, 2007). Then in these media, one can resort to a physical non-equilibrium solute transport formulation that partitions the liquid phase into mobile and immobile regions.

At the study site, the soil contains high percentages of clay, becoming sensitive to preferential flow (Flury et al., 1994; Jarvis, 2007; Greve et al., 2010; Imhoff et al., 2010; Berlin et al., 2013). Consequently, the combination of a single porosity model for uniform equilibrium-type of flow and the mobile-immobile solute transport model (SP-MIM model) was used. Veizaga et al. (2015) showed that this approach was adequate for Cl^- transport at the site. However, it has not been extensively tested for reactive nitrogen species such as ammonium and nitrate as indicated by recent work (Berlin et al., 2013). In FL ammonium is one of the N constituents at high concentrations (Wyngaard et al., 2012). In this work ammonium concentration was simulated as a source of NO_3^-—N production.

2.4.1. Water flow simulation

The spatial and temporal distribution of soil water content and/or pressure head is governed by Richards' equation (Richards, 1931), which reads:

$$\frac{\partial \theta(h)}{\partial t} = \frac{\partial}{\partial z}\left[K(h)\frac{\partial h}{\partial z} - K(h)\right] - S(z,t) \tag{1}$$

where $\theta(h)$ is the volumetric water content [$L^3\,L^{-3}$], dependent on soil water potential expressed as pressure head h [L] both varying in space and time, z is the mean depth positive upward from the water table [L], $K(h)$ is the unsaturated hydraulic conductivity [LT^{-1}], $S(z,t)$ is a sink term representing water uptake by plant roots [$L^3\,L^{-3}\,T^{-1}$], and t is the time [T]. The $S(z,t)$ term can be modeled with alternative formulations. In this work, the Feddes et al. (1974) approach was selected.

The unsaturated soil hydraulic properties were described using the van Genuchten–Mualem functional relationships (van Genuchten, 1980) as follows:

$$\mathrm{Se(h)} = \frac{\theta(\mathrm{h}) - \theta_\mathrm{r}}{\theta_\mathrm{s} - \theta_\mathrm{r}} = \frac{1}{\left(1 + |\alpha \mathrm{h}|^{\mathrm{n}}\right)^{\mathrm{m}}} \tag{2}$$

$$K(h) = K_s S_e^l \left[1 - \left(1 - S_e^{1/m}\right)^m\right]^2 \tag{3}$$

in which S_e is the effective saturation, θ_r and θ_s denote the residual and saturated water contents [$L^3\,L^{-3}$], respectively, K_s is the saturated hydraulic conductivity [$L\,T^{-1}$], α [L^{-1}] is the inverse of the air entry value, n [−] is an empirical shape parameter to the model ($m = 1–1/n$), and l is a pore connectivity parameter [−].

HYDRUS-1D is capable of simulating layered porous media assuming either a vertical, horizontal or inclined direction for the flow domain. In this work, the ROSETTA Lite V1.1 model (Schaap et al., 2001) was used to determine initial estimates for the parameters of the water retention curve, adopting the above formulations for the $\theta(h)$ relationship.

2.4.2. Physical non-equilibrium solute transport simulation: the MIM model

The mobile-immobile water model-(MIM) assumes that non-equilibrium transport (Eq. 5) is caused by physical factors (van Genuchten and Wierenga, 1976; Gerke and van Genuchten, 1993). MIM model used in this work partitions the liquid-phase into distinct mobile (flowing) and immobile (stagnant) liquid pore regions (Eq. 4), and that solute exchange between the two regions can be modeled as a first-order exchange process (Eq. 6 and 7):

$$\theta = \theta_m + \theta_{im} \tag{4}$$

$$\frac{\dfrac{\partial \theta_m c_m}{\partial t} + \partial \rho \bar{c}_m}{\partial t = \dfrac{\partial}{\partial z}\left(\theta_m D^w \dfrac{\partial c_m}{\partial z}\right) - \dfrac{\partial q c_m}{\partial z} - \phi_m - \Gamma_s - S c_r} \tag{5}$$

$$\frac{\partial \theta_{im} c_{im}}{\partial t} = \Gamma_s - \phi_{im} \tag{6}$$

$$\Gamma_s = \omega_{mim}(c_m - c_{im}) \tag{7}$$

$$\bar{c} = k_d c_m \tag{8}$$

where θ_m is the volumetric water content in the mobile phase [L^3L^{-3}] and $\theta_{im}$is the volumetric water content in the immobile phase [L^3L^{-3}]. D^w is the dispersion coefficient [$L^2\,T^{-1}$], q is the volumetric flux density [LT^{-1}], S is the sink term in the flow Eq. (1), c_r is the concentration of the sink term [ML^{-3}], $\Gamma_s$is the mass transfer term in which ω_{mim} is the first-order transfer rate constant for solute between immobile-mobile phases [T^{-1}], $\bar{c}_m$is the solute concentration in the solid phase, and ϕ_m and $\phi_{im}$are reactions in the mobile and immobile domains [$ML^{-3}T^{-1}$]. Its most general interpretation allows any chemical reaction in that phase that leads to losses or gains in the total concentration (Šimůnek et al., 2005, 2008), as follows for NH_4^+—N:

$$\phi_{NH_4^+} = -\mu'_{w,NH_4^+}\theta\ c_{NH_4^+} - \mu'_{s,NH_4^+}\rho\ \bar{c}_{NH_4^+} \tag{9}$$

where μ'_w [T^{-1}] and $\mu'_s$are first-order degradation constants in the liquid and solid phase, respectively, to represent nitrification process from NH_4^+—N to NO_3^-—N (Eq. 9). A similar approach, representing loss of nitrate via denitrification was modeled as a first-order degradation reaction through μ_w [T^{-1}] (Eq. 10).

$$\phi_{NO_3^-} = \mu'_{w,NH_4^+}\theta\ c_{NH_4^+} + \mu'_{s,NH_4^+}\rho\ \bar{c}_{NH_4^+} - \mu_{w,NO3-^+}\theta\ c_{NO_3^-} \tag{10}$$

The nutrient uptake term is the sum of passive and active uptake. The passive component is given by diffusion from the external solution into the cell walls of roots while the active component comprises ion movement from solution to plant against a concentration gradient. Passive nitrate uptake was simulated at plot A, the only site where vegetation grew during fieldwork.

3. Results and discussion

3.1. Soil type

For completeness, a brief description of the soil profile is introduced here. For more details, the reader can refer to Veizaga et al. (2015). At the study site, the soil is classified as a Typic Argiudoll (INTA, 1992). Seven horizons (Table 1) were identified as follows: an A0 organic horizon between 0 and 5 cm, an Ap horizon between 5 and 25 cm, a

Table 1
Soil physical properties.

Soil horizon		A0	Ap				*B*1	Bt1	Bt2	B3	*C*1
Depth (cm)		0–5	5–10	10–15	15–20	20–25	25–37	37–55	55–84	84–106	106–130
Particle fraction (%)	Sand	15.3	24	18.1	17.7	13.8	12.5	4.9	5.5	6.1	5.4
	Silt	36.6	48.2	48.1	46.3	48.3	42.9	39.5	36.5	44.1	46.6
	Clay	48.1	27.8	33.8	36	37.9	44.6	55.6	58	49.8	47.8
ρ_b (g cm^{-3})		0.65	1.07	1.27	1.57	1.37	1.46	1.54	1.58	1.5	1.44
Porosity (e)		–	–	–	–	0.436	0.39	0.4	0.38	0.41	0.4
ρ_s (g cm^{-3})		–	–	–	–	2.56	2.47	2.55	2.54	2.56	2.4
Texture (USDA)		C	CL	SCL	SCL	SCL	SC	C	C	SC	SC

ρ_b. bulk density; ρ_s. real density; SL. silt loam; SCL. silty clay loam; C. clay; SC. silty clay; CL. Clay loam

*B*1 transition horizon 12 cm thick, a Bt1 horizon extending between 37 cm and 55 cm, a B2t horizon extending from 55 cm up to 84 cm, a B3 horizon between 84 cm and 106 cm, and a *C*1 horizon extending from 106 to the bottom of the pit. The Bt horizon is especially relevant for water flow dynamics due to their high clay content. Horizons Bt1and Bt2 (highlighted in Table 1) contain a combined % clay and % silt of around 95%. These fine-textured horizons limit roots development and water/solutes movement within the fine matrix between upper and lower soil layers. However, in this soil by-passing flows may develop thanks to cracks and fissures favoring, in turn, the development of preferential flow paths (Imhoff et al., 2010). Table 1 also shows physical properties of the seven soil horizons identified in the soil pit.

Bulk density increased with depth reflecting reduced organic matter, particles aggregation, and root penetration on subsurface layers, which are also subject to the compacting weight of the soil above them (http://www.nrcs.usda.gov/Internet/FSE_DOCUMENTS/nrcs142p2_053256.pdf).

Compaction is particularly recognizable on the Bt1 and Bt2 horizons. This 47 cm thick layer has a strong to medium angular prism structure that desegregates in moderate to strong angular blocks. It also shows an abundance of slickensides, and it is extremely hard, firm, very plastic and adhesive. Thin roots development occurs through cracks (Veizaga, 2015). These textural and structural characteristics explain the range of bulk density values determined by the cylinder method.

3.2. Soil water chemical characteristics

As mentioned, during the study period between November 30, 2011 and March 30, 2014, a total of 160 soil water samples were obtained. Table 2 shows their distribution by depths and plots.

The analysis of results focused on identifying: 1) quantitative differences between plots, 2) vertical variations of mean values and range corresponding to each variable of interest EC, Cl^- and NO_3^-—N.

Fig. 2 shows measurements of selected physicochemical parameters at the three plots. Instead of the classical box-type plot the data cloud was drawn to visualize the dispersion of data values. The center square represents the parameter mean, the "whiskers" on the left and the right of the solid line show the location of the minimum and maximum. At each plot, the mean EC value was relatively uniform along the profile, pointing out that salts are transported from upper layers to lower layers with little alteration. However, its magnitude remarkably differs from plot to plot according to different degrees of exposure to feedlot effluents. Plot A registered the lowest EC values, presenting mean values $<1500\ \mu S\ cm^{-1}$ for all depths (except at 1 m). At plot B, mean EC values at different depths increased, lying between 1900 $\mu S\ cm^{-1}$ and 2400 $\mu S\ cm^{-1}$. Notice that at this plot the EC values range was higher at 30 cm depth than at other depths. Plot C, the most impacted site, showed EC values higher than at plot A and plot B, with mean values between 5100 $\mu S\ cm^{-1}$ and 6350 $\mu S\ cm^{-1}$ at different depths.

Table 2
Number of collected soil water samples classified by plot and depth.

Depth [cm]	Plot A	Plot B	Plot C	Total
30	19	23	10	52
60	14	25	11	50
75	13	–	7	20
100	9	16	13	28
Total	**54**	**64**	**42**	**160**

The contrast of EC values between plots is attributed to the impact caused by different flows of the water-manure solution on each them. As it will be shown later, water and solutes flow at plot A were governed by a combination of dry and wet cycles under unsaturated conditions, while at plot B and plot C near-saturation conditions even the range of EC variation at each depth. Nonetheless, it is possible to identify quantitative differences between plot B and plot C as a consequence of water-manure solution deposition on the surface.

The Cl^- ion is a main contributor to EC (Veizaga et al., 2015). In general, patterns of Cl^- concentration showed an increase with depth, except at plot C where the behavior of Cl^- was very similar to that of EC.

Evapotranspiration processes seem to be relevant at plot A where roots development was abundant up to 30 cm, therefore contributing to the observed variability in Cl^- concentration values (masked in the figure due to the concentration scale used to enclose all the observed values to differentiate behaviors among plots). Successive precipitation events washed the profile transporting Cl^- to deeper horizons through either the soil matrix and/or preferential flow paths. At plot C, devoid of vegetation, Cl^- is carried from the surface source (lagoons overflows) into the soil profile virtually without alteration.

Patterns of NO_3^-—N concentrations are notoriously different from EC and Cl^-, Ranges and distribution of NO_3^-—N with depth differ from plot to plot, suggesting not only variations of pollution exposure at the soil surface but also the occurrence of different transformation processes within the soil profile. At plot A, vegetation nutrient uptake reduces NO_3^-—N concentration at 30 cm. Soil texture and the underlying hydrology of this plot may explain observed concentrations. The 60 cm depth observation point is located within the Bt2 horizon [55–84 cm], which contains 58% of clay, is very hard, very adhesive and plastic. The textural contrast between this and the upper horizon could limit water flow under unsaturated conditions. However, higher NO_3^-—N concentration were observed at lower horizons. Successive precipitation events may transport nitrate to deeper horizons through either the soil matrix and/or preferential flow paths.

High NO_3^-—N concentrations were measured at 30 cm at plots B and C, reducing considerably with depth. This behavior seems to respond to the hydrology of the sites and exposure to effluents: (1)- near-permanent presence of manure and/or manure-solution deposited on the vicinity of the monitoring site transported by surface runoff from FL pens (plot B) and lagoons overflows (plot C), and (2) saturated conditions of shallow depth horizons for long periods after precipitation events.

Field results suggest that unlike Cl^-, the observed variability of NO_3^-—N concentration values among plots and depths are the result of different controls at each site. The NO_3^-—N distribution at plot A challenges the traditional idea of a textural control due to the presence of a hard, plastic Bt2 horizon that could limit water and nitrate movement to

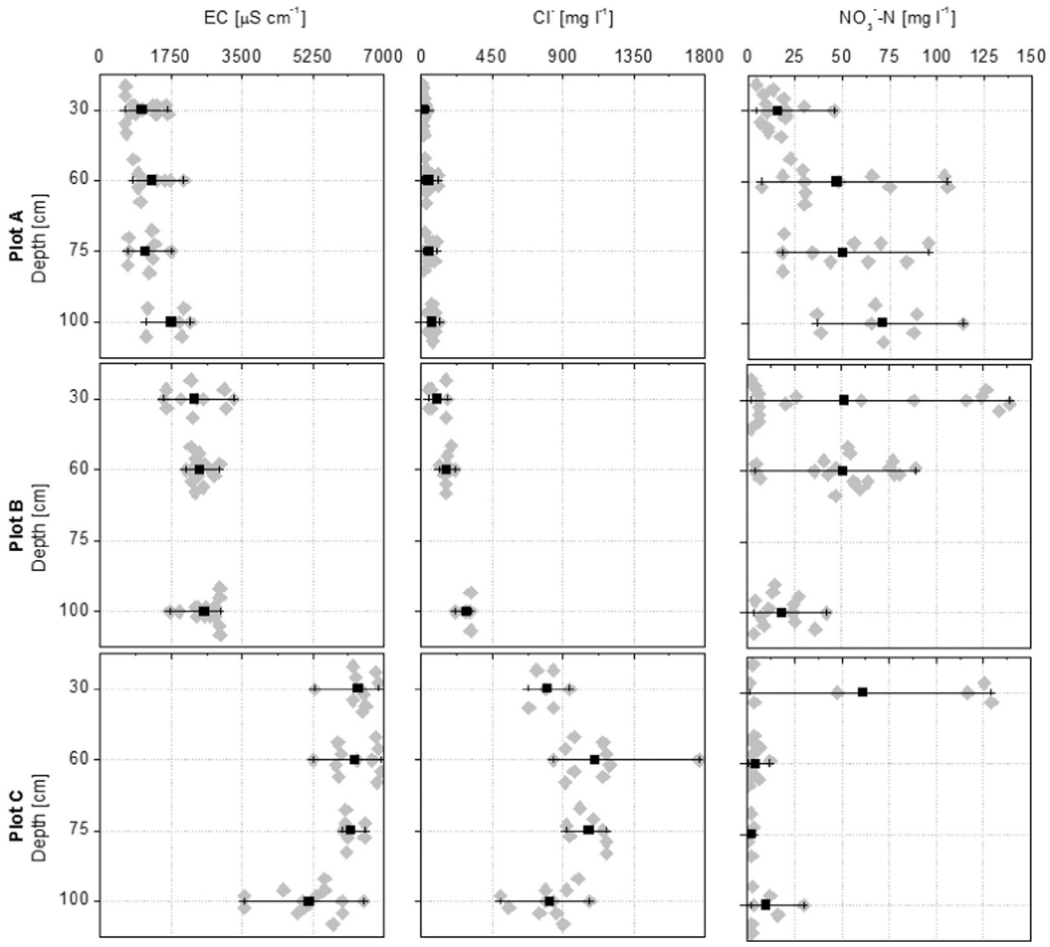

Fig. 2. Concentration of EC, Cl^- and NO_3^-—N corresponding to plot A, plot B and plot C at different depths. All collected data were used to construct the diagrams.

deeper soil layers. Veizaga et al. (2015) showed that Cl^- distribution at plot A could be partially explained by the presence of cracks typical of fine-textured material that resulted in increasing Cl^- concentrations with depth.

Plot B is frequently affected by ponded water–manure solution accumulated after precipitation events, becoming a relevant salt source. Its chemical characterization can help explain the occurrence of higher Cl^- concentrations and EC since vegetation has no influence on this plot, suggesting the potential importance of lateral subsurface flows. However, in plots B and C, contrary to plot A, prevailing saturated conditions in deep soil horizons and fluctuating saturation conditions at the surface soil layers, can promote and trigger biological processes related to the N cycle. The potential for both source and sink of NO_3^-—N at different depths of the soil profile suggested by the data will be assessed by numerical simulations.

A discussion on primary sources of N at the site is merited at this point. Feedlot and dairy operations effluents have similar components. According to Baram et al. (2012b), seepage water from earthen dairy waste lagoons contains high quantities of organic-N and NH_4^+—N, whereas in the subsurface, nitrate (NO_3^-—N) is the most common contaminant. Oxidation of ammonia (NH_3) and NH_4^+ into NO_3^-—N (nitrification) in porous medium carried out by bacteria requires a source of molecular oxygen (O_2) (Prosser, 1989) and carbon. Nitrate can be further reduced by microorganisms into N gas (N_2) through denitrification. In fine-textured soils affected by desaturation-saturation episodes such as those present at the study site, both nitrification and denitrification could occur. This process is called coupled nitrification–denitrification (CND) (Kremen et al., 2005; Baram et al., 2012a). It is acknowledged that oxygen and organic carbon concentrations can strongly affect nitrate dynamics. In FL environments, organic carbon is not a limiting component for microbial activity, however the available O_2 can enhance nitrification while limiting denitrification, in turn affecting nitrate dynamics. Although the measurements did not consider oxygen and organic carbon concentrations, an attempt was made via modeling, to represent CND with a similar approach as that used by Ramos et al. (2012). assuming that neither C nor O_2 was limiting for microbial activity.

3.3. Soil moisture and hydrochemical patterns over a wet period

A selected period was isolated for a detailed analysis of the concentration data to identify processes that may be masked in an integrated, lumped analysis. A wet period between October 6, 2012, and December 23, 2012 (i.e. a 73 days period), recorded a cumulative precipitation of 571 mm that represents 49% of the average annual precipitation for the region (series 1971–2013). For completeness, a brief description of the water movement through the soil profile is presented to inform the reader before the use of the numerical model to interpret observed NO_3^-—N concentrations at each plot.

3.3.1. Pressure head variation

The variation of pressure head at plot A in response to atmospheric forcing given by precipitation and evapotranspiration is shown in Fig. 3. Pressure head ranged from 0 KPa (saturated soil) to 70 KPa at all depths denoting a relatively wet profile. The first sensor (30 cm) registered a systematic quick response to precipitation reaching saturation immediately after each event, followed by a consistent linear drying process always occurring at a similar rate. The sensor at 60 cm, located

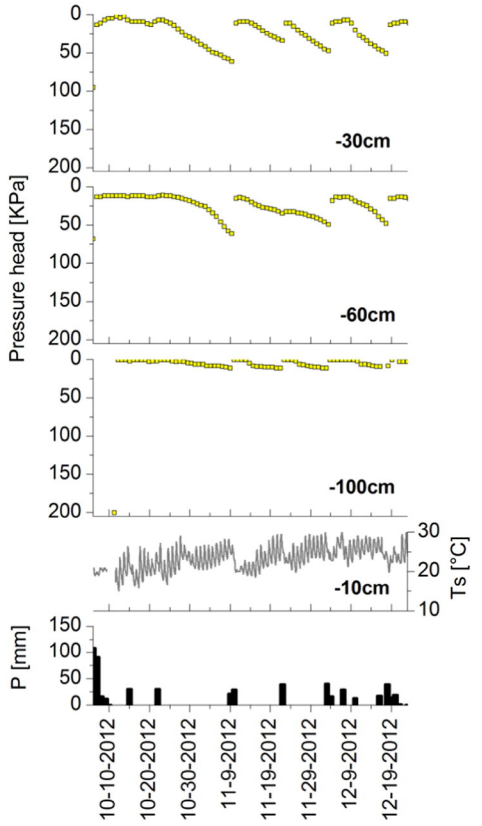

Fig. 3. Pressure head at different depths, soil temperature (Ts) at 10 cm depth and daily precipitation (P) measured at plot A from October 6th, 2012 to December 23th, 2012.

within a denser horizon, responded rapidly to moisture fronts but only for cumulative precipitation of >50 mm, although the drying process was different. Differences in pressure head response at these two depths could be mainly explained by (1) the presence of abundant vegetation roots at 30 cm depth that contributes to evapotranspiration, and (2) fewer roots and textural characteristics of the heavy soil horizon at 60 cm that could slow the drying process. In contrast to the upper layers, at 100 cm depth, measured pressure head lied between 0–20 KPa. Values were relatively stable, remaining at near-saturation conditions during the analysis period, denoting a notable water-holding capacity. Sub-surface soil temperature records showed an increasing seasonal trend as summer days approached. Daily fluctuations of about 10 °C were measured with a significant temperature drop on rainy days. Identifying pressure head patterns at different depths will partially help interpret hydrochemical responses to precipitation events.

3.3.2. Hydrochemical response

A wet soil profile facilitated soil water sample collection. Five 2, 3 and 4-day field campaigns were undertaken during the wet period [October 6, 2012 - December 23, 2012]. Fig. 4 shows measured EC, Cl^- and NO_3^-—N concentrations at plot A and plot B. Abundant rainfall occurred in the second half of the analysis period, resulting in dilution of Cl^- at plot A, even at 100 cm depth. However, significant dilution was not observed at plot B. Plot B is located at a slightly lower elevation than plot A (in the order of 50 cm), which in turn, favors surface flow and accumulation of water/manure nearby. Ponded water may induce subsurface, high-salt concentration due to lateral flows, which could explain relatively constant EC and Cl^- concentrations at plot B during this period.

Temporal and spatial variations of measured NO_3^-—N concentrations did not exactly follow the aforementioned patterns. At plot A the trend of NO_3^-—N concentrations was similar to that observed for Cl^- and EC however, concentration values at different depths were bracketed within a narrower range. In contrast, at plot B, NO_3^-—N concentration increased in the upper layers towards the end of the analysis period which may be an indication of nitrification. Another interesting observation is that NO_3^-—N concentration values decrease significantly with depth between the first days and last days of the analysis period, suggesting that denitrification may be occurring.

Due to operational constrains and accessibility issues, no concentration data were available for plot C for the selected wet period.

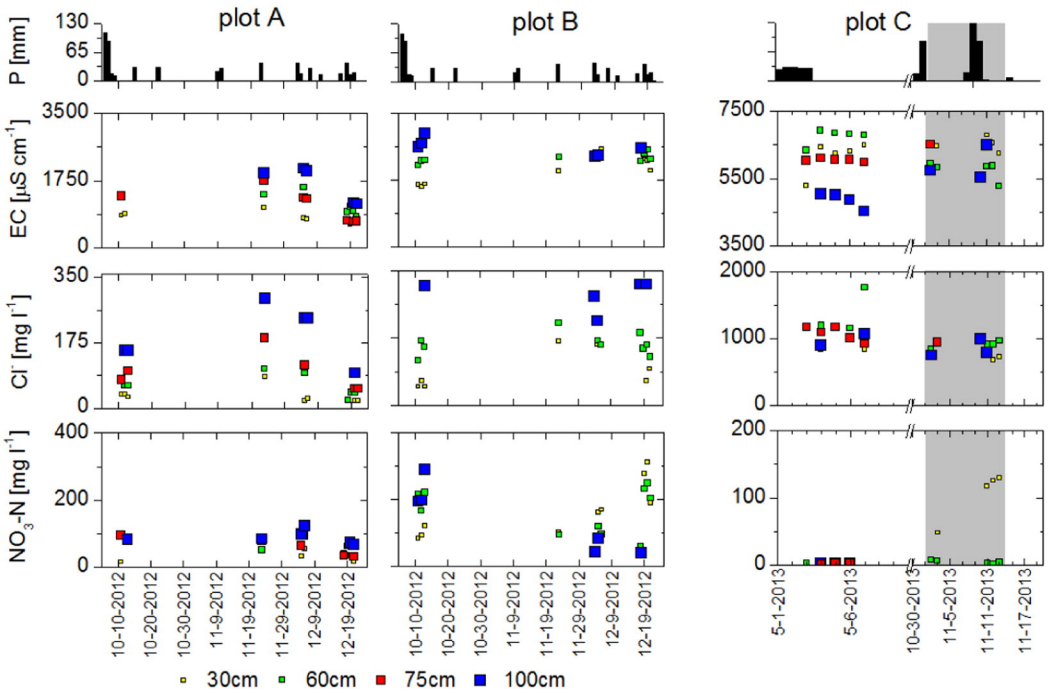

Fig. 4. Space-time variation of EC, Cl^- and NO_3^-—N concentrations in response to rainfall during a wet period. Data at plot A and plot B correspond to period October 6–December 23, 2012, data at plot C correspond to period May 1–November 20, 2013.

Nonetheless, for completeness and comparison between the three sites, a different period was analyzed from May 1, 2013 to November 20, 2013 (Fig. 4). The temporal pattern of EC values was similar to that observed at plot B. Chloride concentration values showed little differences at depths however they decreased with time, with concentrations around of 1000 mg l^{-1} at all depths. However, NO_3^-—N concentration values were the lowest among plots for the deeper horizons with the exception of an increase recorded at 30 cm after the October 30th rainfall (maximum concentration of 150 mg l^{-1}), in agreement with the observed dynamics at plot B.

From the above results, it is clear that NO_3^-—N dynamics and distribution in the soil profile is complex at the field site. Numerical modeling may guide identifying additional processes affecting its transport and transformation exploring the range of transformation constants that may apply to the site.

3.4. Simulation for nitrate transport over the wet period

3.4.1. Model setup

The one-dimensional flow and solute transport domain extended up to a depth of 130 cm, divided into four layers (Table 3) and discretized with 261 nodes densified near the soil surface. Observation nodes were defined at depths corresponding to the location of suction cups. The same soil profile was used for all three plots. Boundary conditions for water flow were set as follows: a) atmospheric conditions at the soil surface; b) free drainage at the bottom of the simulated soil profile at plot A, constant pressure head at the bottom of plot B and plot C.

For simulating solute transport under variably-saturated flow conditions, the combination of single porosity water flow with mobile-immobile solute transport (SP-MIM) was used (Glaesner and Gerke, 2013). The simulation period extended for 73 days corresponding to the wet period described in Section 3.3. A flux concentration type boundary condition was set at the soil surface while a zero concentration gradient was defined at the bottom of the profile.

Initial conditions profile for EC, Cl^- and NO_3^-—N were defined by the observed concentration at the first simulation day. Ammonium concentration in the incoming water was equal to 0.01 mg cm^{-3} for plot A, 0.1 mg cm^{-3} for plot B and C. The increment of concentration value tend to represent the degree of exposure to ammonium at each site.

Initial conditions for ammonium in the mobile and immobile zones were set with a linear declining trend from the concentration at surface up to 0 mg cm^{-3} at 40 cm deep for plot A, plot B and plot C.

Table 3
Optimized hydraulic and solute transport parameters for each layer in the model simulation for plots A, B, and C.

Parameter	Layer 1 [0–15 cm]	Layer 2 [15–37 cm]	Layer 3 [37–84 cm]	Layer 4 [84–130 cm]
Θ_r [cm^3 cm^{-3}]	0.0588	0.0640	0.0699	0.0704
Θ_s[cm^3 cm^{-3}]	0.4743	0.4022	0.3900	0.4135
α [KPa^{-1}]	0.0180	0.0063	0.0042	0.0160
n [−]	1.3527	1.1540	1.1500	1.2050
K_s [cm d^{-1}]	29.63	9.23	6.84	10.77
l [−]	0.5	0.5	0.5	0.5
D_L [cm]	30.00	8.70	21.40	3.72
Θ_{im}[cm^3 cm^{-3}]	0.10	0.30	0.32	0.32
ω [d^{-1}]	0.008	0.003	0.003	0.008
D_o [cm^2 d^{-1}]	1.7	1.7	1.7	1.7
Reaction parameters for plot A, B and C:				
$\mu'_{w,\ NH4+}$ [d^{-1}]	0.2	0.2	–	–
$\mu'_{s,\ NH4+}$ [d^{-1}]	0.2	0.2		
K_d [cm^{-3} g^{-1}]	3.5	3.5		
First-order rate to denitrification process for plot B and C:				
$\mu_{w,\ NO3-}$ [d^{-1}]	–	–	0.1	0.1

3.4.2. Calibrated parameters

As previously mentioned, all model parameters depending on textural characteristics for each horizon (Θ_s, Θ_r, α, n,) as well as the saturated hydraulic conductivity K_s and the pore connectivity parameter l were initially estimated using the model ROSETTA Lite Version 1.1, available in HYDRUS-1D (Schaap et al., 2001).

In ROSETTA, the retention curve and the hydraulic conductivity curve are constructed using soil data from agricultural and non-agricultural lands of the northern hemisphere (Schaap and Leij, 1998a, 1998b). Therefore, their representativeness for Argentinean soils may be questioned. The initial parameter values were later adjusted during calibration using HYDRUS-1D inverse routine using local parameter values for the study area (Imhoff et al., 2010). Table 3 shows fitted hydraulic and solute transport parameters for all layers considered in the model simulation.

Calibrated hydraulic parameters are consistent with soil texture. Although each parameter has a clear physical sense, van Genuchten and Nielsen (1985) noted that Θ_r and α often have an empirical character. In spite of this observation, an attempt was made to compare the range of calibrated values with those reported in the literature for similar soils. Values of hydraulic parameters for coarse to medium texture soils are commonly reported in the literature (Santini et al., 1995). However, values for fine-textured soils are rarer (Ventrella et al., 2000; Imhoff et al., 2010). The α-coefficient reduced from 0.018 for layer 1 (average 20% sand) to 0.0063 and 0.0042 for layer 2 and 3, respectively (average 5% sand), in tune with the expected increase in air entry value associated with finer-textured materials.

Saturated hydraulic conductivity Ks reduced threefold between the coarsest, upper layer, and the finest, lower layers, from near 30 up to 6.84 cm d^{-1} for layer 3. This latter value is similar to that reported by Ventrella et al. (2000), equal to 5 cm d^{-1}, for a very fine-textured material. But it differs from the typical Argiudol described by Imhoff et al. (2010), who mentioned field estimates of Ks equal to 168 cm d^{-1} on a parcel labored with direct sowing.

Fieldwork was performed during and after precipitation events, being difficult to characterize runoff water, which in turn, becomes infiltrating water into the soil. The solute concentration of the incoming water is an input to HYDRUS-1D. Consequently, this variable was considered a calibration parameter due to the impossibility of measuring chemical components of surface runoff in real-time, becoming a source of results uncertainty.

Model transport parameters were fitted using the Standard Mode option within HYDRUS-1D (Šimůnek et al., 2005). Due to the inability to measure transport parameters or to rely on published values for similar soils for comparison purposes, calibrated parameter values are uncertain. Also, it is recognized that the multiple parameters combinations can lead to a non-unique result. Previous results from a sensitivity analysis performed to ascertain Cl^- transport model response to certain parameters changes, indicated that simulated Cl^- concentrations were not sensitive to D_L, D_o and ω (Veizaga et al., 2015). However, they were sensitive to the value of Θ_{im} showing the model dependency on immobile water availability to reproduce adequately observed Cl^- concentrations. This dependency also supports the use of the MIM approach for solute transport in the studied soil. A new sensitivity analysis was conducted to explore uncertainty in the selection of the new parameters.

In this work, $\mu'_{w,NH4+}$ and $\mu'_{s,NH4+}$ were assumed equal to 0.2 d^{-1} and ammonium was assumed to adsorb to the solid phase using a distribution coefficient Kd of 3.5 cm^3 g^{-1}, which represents the center of the range of values reported by Hanson et al. (2006). Volatilization of ammonium and subsequent ammonium transport by gaseous diffusion was neglected (Ramos et al., 2012). Besides nitrogen species, Cl^- and and EC were simulated.

3.4.3. Simulated hydrochemical variables

Measured and simulated pressure head for plot A are presented in Fig. 5 (top panel), showing an adequate fit of observed data. The same

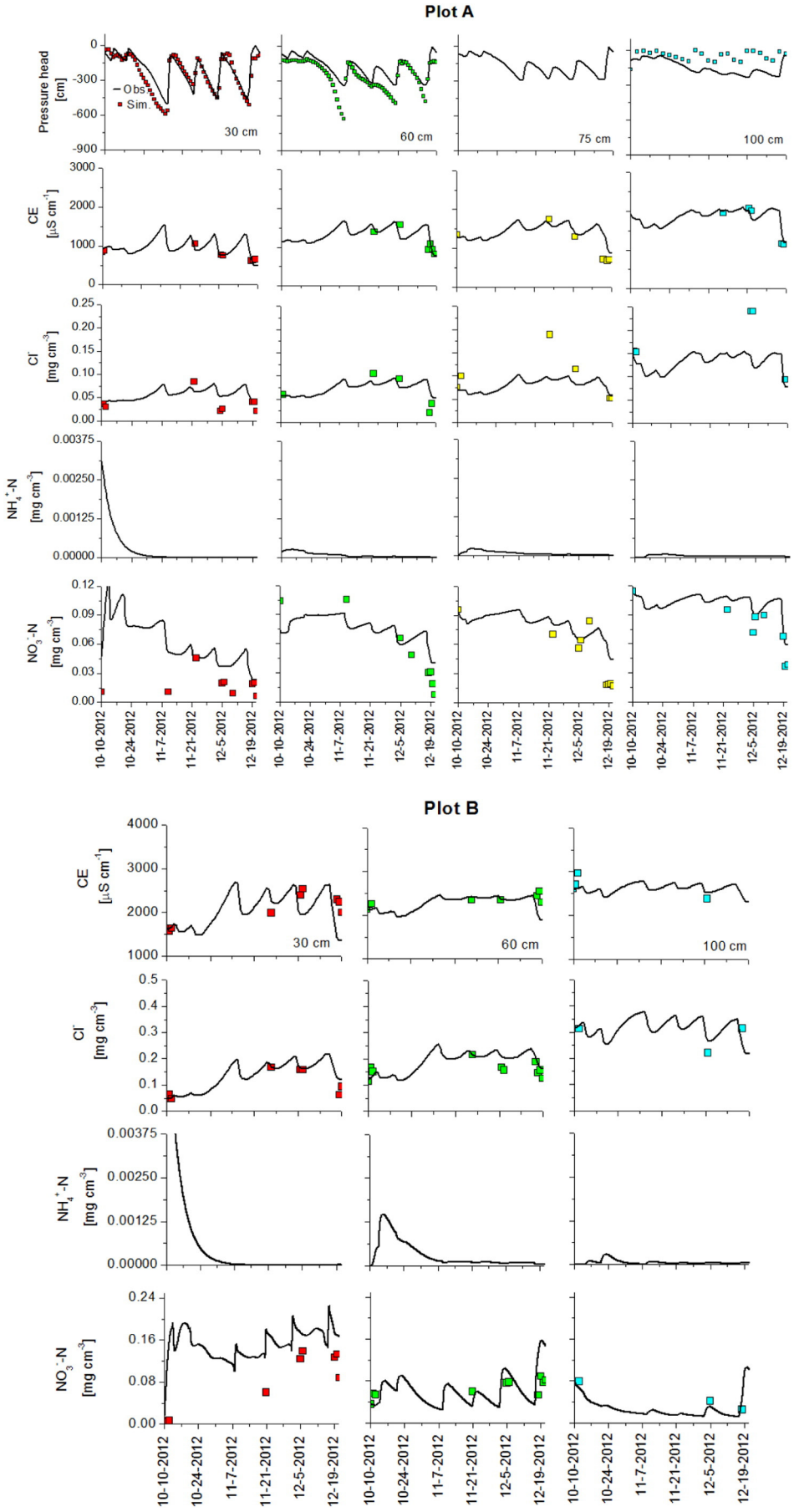

Fig. 5. Comparison between measured and simulated EC, Cl^- and NO_3^--N values and concentrations at plot A and plot B at different soil depths.

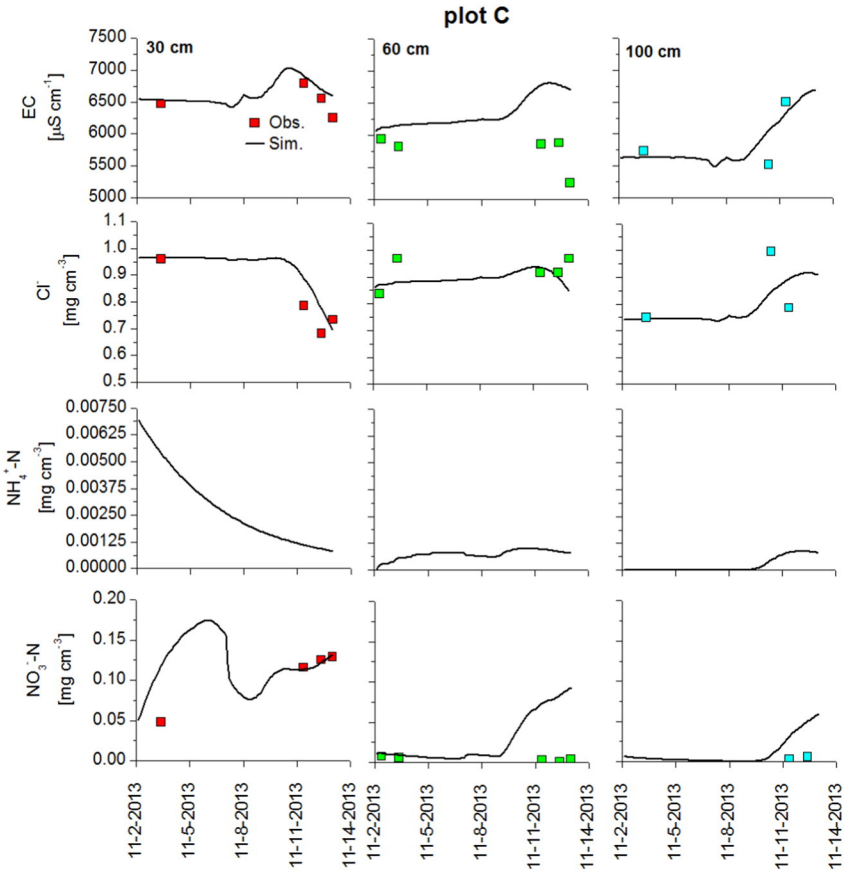

Fig. 5 (*continued*).

figure shows measured and simulated values of CE, Cl^- and NO_3^-—N at plot A, plot B and plot C. Also included are simulated concentrations of NH_4^+—N at plot B and C.

At plot A, simulation results satisfactorily matched measured data. As a result of precipitation events, solute concentrations (EC, Cl^- and NO_3^-—N) undergo a sharp decline at all depths. Infiltrated water dilutes salts along the profile transporting them to deeper horizons, in agreement with recent findings reported in the literature (Ramos et al., 2012). On the contrary, between precipitation events measured/simulated pressure head (suction) increases as a result of high evapotranspiration rates, which in turn, causes the concentration of salts near the soil surface. This effect progressively dissipates at deeper soil layers. Note that NO_3^-—N uptake by plant roots was activated at plot A.

Even though measured ammonium concentrations were not available for comparison with simulated results, the model would indicate that NH_4^+—N is rapidly nitrified and NO_3^-—N transported into lower layers. Previous results supported the use of the MIM approach for Cl^- transport in plot A. These new results reassure the suitability of this model not only for Cl^- but also for CE and nitrate.

To a large extent, at plot B measured values of EC and Cl^- concentrations remain stable with depth, a pattern that the model reproduces correctly. The combination of adequate moisture levels, hot temperatures and the abundance of organic material at surface layers result in suitable conditions for nitrification in both plot B and plot C. Similar to plot A, model simulated NH_4^+—N is rapidly nitrified and NO_3^-—N transported into lower layers. However, the particular characteristics of plot B and C (saturated conditions in deep soil layers) may trigger denitrification. This process was simulated as a first-order reaction at the two deepest layers of the model with $\mu_{w,NO3-} = 0.1d^{-1}$ (Smith and Tiedje, 1979).

The simulated NO_3^-—N concentration at plot B adequately reproduced measured data, slightly overestimating at 30 cm depth. Ammonium is rapidly converted to NO_3^-—N at upper layer, Nevertheless, a measurable concentration is transported downward and detected at 60 cm deep. Again, the saturated conditions are favoring vertical transport.

At plot C, data availability limited solute transport simulations and comparison with the other plots. On the one hand as explained, the site late instrumentation precluded relying on a data set concomitant with plot A and B. On the other hand, during humid periods accessibility to plot C was restricted due to lagoons overflowing and muddy conditions, interfering data collection activities. Nonetheless, a simulation was attempted for a very humid period from November 1, 2013 to November 13, 2013, where cumulative rainfall reached 233.7 mm, to test the performance of the modeling approach at this impacted site. Measured and simulated values of CE, Cl^- and NO_3^-—N are shown in Fig. 5. Modeled NO_4^+—N is also included in the figure. Simulation results satisfactorily matched measured solute concentrations at 30 cm. Interestingly, observed EC and Cl^- values decreased at the end of the simulated period at the upper layer, probably because of intense dilution processes caused by the extreme precipitation event. Contrary, observed NO_3^-—N concentrations increased. However, the model did not succeed at reproducing observed nitrate concentrations at 60 cm and 100 cm. Low concentration measured data could be attributed to lateral, subsurface flow coming from the unlined retention lagoons located upstream of the site. This flow may have encountered a quite dense horizon which impeded downward movement. More field data should be collected in future studies to confirm this hypothesis and modeling results at this location.

It is acknowledged that a source of uncertainty of model results is the concentration of incoming water (C_{TOP}), a HYDRUS-1D input data, which is unknown in this case. Within the simulated twelve-day-period, precipitation was distributed as shown in the shaded area of Fig. 4. According to field observation, during the first day of heavy precipitation,

lagoons overflow spread all over the surrounding land in a mantle-type manner. On the second day of heavy precipitation, overflows concentrated within carved, run-off channels by-passing the monitoring plot C, rendering very complex the estimation of C_{TOP}.

3.5. Model goodness of fit

Flow and transport model performance was assessed quantitatively by means of various criteria applied to pressure head and concentrations, respectively. The following statistical measures of goodness of fit (Zheng and Bennett, 2002) compared field measured values with HYDRUS-1D simulations. Quantitative measures of uncertainty were the mean error (ME), mean absolute error (MAE) and root mean square error (RMSE), expressed as:

$$ME = \frac{1}{N}\sum_{i=1}^{N}(O_i - P_i)$$

$$MAE = \frac{1}{N}\sum_{i=1}^{N}|O_i - P_i|$$

$$RSME = \sqrt{\frac{\sum_{i=1}^{N}(O_i - P_i)^2}{N-1}}$$

where O_i and P_i are observation values and model results in the units of the particular variable, respectively, and N is the number of observations. The subscript i indicates observation number, while the term in parentheses is called model error.

Model results closely replicate pressure head at plot A. The statistical indicators (Table 4) integrate results for three depths resulting in a ME of −0.0021 cm, a MAE of 0.0452 cm and a RMSE of 0.0564 cm. Numerical results of the continuous overall soil water salinity characterized by EC produced an RMSE of 0.0635 μS cm^{-1} for plot A and 0.0801 μS cm^{-1} for plot B, which indicate an acceptable model performance comparable to errors reported from HYDRUS-1D simulations performed by Ramos et al. (2011) and even HYDRUS-2D simulations by Ramos et al. (2012). It would be desirable to rely on a higher number of observation data to obtain more robust statistical indicators for hydrochemical variables. The use of ceramic cups difficulted soil solution sampling during dry periods, reducing in turn, the number of data points for model calibration and statistics estimations. Nonetheless, N was higher than 22 in all calculations included in Table 4.

3.6. Model sensitivity

Normalized sensitivity coefficients $\kappa_j$were calculated to test the overall responsiveness and sensitivity of the model results to certain input parameters. The coefficient $\kappa_{i,j}$ is defined as the ratio of relative variation in the output variable y to relative variation in parameter input values a_j, as follows:

$$\kappa_j = \frac{\partial y / y_0}{\partial a_j / a_{j0}}$$

Where y_0 is the output variable calibrated value, and a_{j0} is the value of the j_{th} parameter of the reference/calibrated simulation run, respectively. These normalized sensitivities are dimensionless quantities that can be used to compare the importance of different observations to the estimation of a single parameter or the importance of different parameters to the calculation of a simulated value (Hill, 1998). In this work, they were used for this second purpose, focusing on transport parameters.

Counting the four layers, and three investigation sites, the number of parameters candidates to be tested would be quite large. As mentioned in Section 3.4.2, results from a previous sensitivity analysis performed to ascertain Cl— transport model response to certain parameters changes, indicated that simulated Cl— concentrations were not sensitive to DL, Do and ϖ. Based on the calibration stage, and to simplify the analysis, the target output variable is the simulated nitrate concentration in the top layer of plot B because of the variety processes occurring at that site. Among candidate parameters to conduct sensitivity analysis, the partition coefficient Kd and the concentration of ammonium in the incoming water C_{TOP} were investigated. Values of the calibrated parameters used in the denominator of the above equation are given in Table 3.

A model is said to be sensitive if $\kappa > 1$, neutral if $\kappa = 1$, and robust if $\kappa < 1$ (Rodríguez et al., 2008). Normalized sensitivity coefficients for each K_d tested shown in Fig. 6 corresponds to the mean κj for the simulation period. For the range of tested Kd, κ was between 0.207 to 0.212, a relatively uniform value less than one, indicating that model results were not very sensitive to Kd. The range of tested distribution coefficient was between 1.5 and 4 $cm^3\ g^{-1}$, defined by Hanson et al. (2006) from previously published values.

The normalized sensitivity coefficient for C_{TOP} depicted in Fig. 6 corresponds to the mean κ for the simulation period. The coefficient values were less than one but above κ for K_d parameter. The concentration of incoming water is a site dependent variable related to mechanisms that affect the source at each site. For lower values of C_{TOP} (NH_4^+—N), between 0 to 0.125 mg cm^{-3}, κ remains constant equal to 0.338. Larger values of C_{TOP} cause a rapid increment of κ denoting the incipient sensitivity of model results to the concentration of incoming water.

Table 4
Results of the statistical analysis between measured and simulated pressure head at plot A, and measured and simulated EC, Cl^- and NO_3^-—N concentrations at plot A and B.

Statistic	Pressure head (cm)	EC (uS cm^{-1})	Cl— (mg cm^{-3})	N—NO_3— (mg cm^{-3})
Plot A				
N	219	25	26	34
ME	−0.0021	0.0263	4.42E-6	−3.38E-6
MAE	0.0452	0.0515	7.57E-6	5.82E-6
RMSE	0.0564	0.0635	1.19E-5	7.45E-6
Plot B				
N	–	24	22	23
ME	–	0.0423	6.82E-7	−2.55E-6
MAE	–	0.0552	2.70E-6	4.63E-6
RMSE	–	0.0801	3.66E-6	6.62E-6

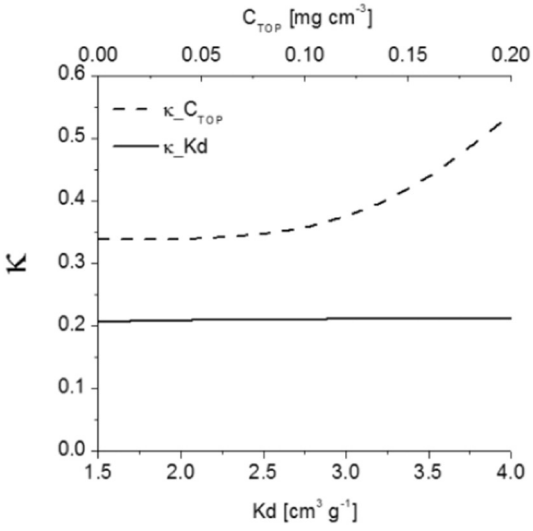

Fig. 6. Sensitivity analysis for K_d parameter and the incoming concentration of ammonium (C_{TOP}) at plot B.

Interestingly, Chevron and Coquet (2008) conducted a sensitivity analysis of transient-MIM HYDRUS-1D evaluating the ratio of relative variation in output pesticide concentration to relative variation in parameter input values. The authors found that transient MIM HYDRUS-1D was highly sensitive to parameters related to pesticide degradation and sorption, especially the Freundlich exponent associated with nonlinear sorption.

3.7. Model deviation from data

Deviations between measured and simulated variables expressed by error calculations presented in Table 4 can be attributed to different causes, including errors related to field measurements, modeling approach, model structure and model inputs. A brief discussion of each of them follows.

3.7.1. Measured data

Pressure head sensors measure bulk soil moisture, i.e. moisture contributed by mobile and immobile water alike, in proportions that will depend on the soil moisture condition. For instance, one could speculate that if the sensor is located at or near a crack formed after a drying period, it would measure mobile water after the first rain. If the soil moistens enough so as to close small cracks, then the sensor would measure predominantly immobile water. As presented in Köhne et al. (2009), the acceptable of the single porosity model performance achieved here with meaningful physical soil parameters has been reported in previous studies. These authors also highlighted the limitation in using flow data alone for the identification of dual porosity models parameter and the role of preferential flow in structured soils.

Since it was difficult to collect soil solution samples with ceramic cups during dry periods, model simulations could not be compared with measured data during these periods. Therefore, measured-simulated comparison is restricted to wet periods. Besides, concentrations determined from suction cups samples represent both spatial and temporal averages while they are compared against point and time-specific simulated values. The sampled volume depends on soil hydraulic properties, soil moisture content and applied suction (Weihermüller et al., 2005, 2011). Even though three distinct data collection sites around lagoons effluents were investigated, spatial soil variability can also affect concentrations measured by suction cups, a topic extensively investigated by Weihermüller et al. (2011). Likewise, the number of field measurements differed from plot to plot, affecting simulations robustness where few calibration measurements were available, namely plot C.

3.7.2. Modeling approach

3.7.2.1. MIM model. Based on van Dam et al. (1990) and Ventrella et al. (2000) experience, the MIM approach combined with the single porosity Richards' equation was used in this study. For consistency, the same SP-MIM model was implemented for all three plots. Adopting the MIM approach improved transport results at plot A (Veizaga et al., 2015), where cracks and macropores may develop. Pressure head data were available at this site to identify rapid responses (associated to by-passing flows)/slow responses (associated to matrix flows). Improvement of concentration results was not so evident at plot B and C, probably because of the near-saturation conditions of the soil profile at these sites, creating a different flow-transport environment.

3.7.2.2. Nitrate species simulation. In soil-groundwater systems, nitrogen species consist of NH_4^+—N, NO_3^-—N, organic N and nitrogen gas (N_2). The transformation from one species into another will depend on environmental conditions, particularly pH, temperature, oxygen and microorganisms activity. In this work, the modeling approach to transport N species, namely NH_4^+—N and NO_3^-—N, used first-order reactions to represent nitrification-denitrification processes. This type of representation was successfully used in studies by Johnsson et al. (1987), Mailhol et al. (2007), Crevoisier et al. (2008) and Ramos et al. (2012). Alternatively, full monod kinetics could be used to model N-transformations (Lee et al., 2006).

3.7.3. Model structure

3.7.3.1. 1D vs 2D. Ramos et al. (2012) compared their two-dimensional results with one-dimensional results of the same study site, concluding that adopting the 2D approach proved to be beneficial in lowering the simulation errors. Nonetheless, the same authors stressed that the notion of increasing model dimensionality, in their case to three-dimensions, do not necessarily bring a better match between measured and simulated data. In their own experience, NO_3^-—N— simulated concentrations were worse.

Field data at plot B and C suggested the possible occurrence of subsurface, lateral flows. Exploratory simulations with HYDRUS-2D software package (Šimůnek et al., 2006) were attempted (Veizaga, 2015). The 2D configuration included plot B and surrounding areas, and extended to the ponding area nearby, suspected to cause subsurface flows after heavy rains. Model runs were constrained by limited data, providing uncertain results. The simulations were kept as simple and rigorous as possible to comply with the objectives of comparing the three sites.

3.7.3.2. Layer discretization. A four-layer discretization was adopted for the representation of the soil profile grouping similar horizons identified in the soil pit where observation points were located. However physical properties and textural characteristics allowed describing seven horizons. Even though, it is considered an adequate discretization compared to similar HYDRUS-1D simulations (Ramos et al., 2011; Saso et al., 2012). More critical could be the fact that the same calibrated hydraulic parameters were used at the three plots given the constrain of pressure head data availability. As discussed, the surface exposure to runoff is may differ from site A, B and C.

3.7.4. Model input data

3.7.4.1. Initial conditions concentration. Initial condition for EC, Cl^- and NO_3^-—N was known, it was not for NH_4^+—N. Based on measured NO_3—N and considering the N-species transformation processes in these environments (Lee et al., 2006), a linear decaying NH_4^+—N profile was assumed, with the underlying hypothesis that has underwent nitrification prior to the simulated period.

4. Summary and conclusions

This work documented the NO_3^-—N dynamics and its migration in a fine-textural soil impacted by feedlot (FL) operations representative of the Argentine Pampas region. Findings of this research increased the understanding of fundamental processes leading to the observed NO_3^-—N dynamics that can assist management strategies to mitigate the negative impact on surrounding environments.

Key outcomes were the result of a careful selection of monitoring sites (plots A, B, and C) subject to different degrees of exposure to manure accumulation and lagoon overflows following significant rainfall events, confirming recent findings elsewhere from beef-dairy farms enterprises under heavy texture soils. Site selection was a relevant factor, allowing field-oriented activities under budget constraints like those found in developing countries.

Both statistical analysis over the entire dataset and numerical modeling over a wet period were undertaken. Results from both methodologies pointed out that the combination of different hydrological conditions and exposure (and duration) to manure on the soil surface have a profound impact on the transport and transformation of NO_3^-—N in the soil profile, which overshadowed the expected

structural control by the B2t horizon (clay). The model confirmed that NO_3^-—N and Cl^- reached deep horizons (up to 1 > m) at FL locations with less exposure to manure, vegetation grow, and prevailing unsaturated soil conditions driven by climatic forcing. This finding is significant, and further supports recently published works challenging the traditional idea that fine-texture soils mostly act as an impeding layer for NO_3^-—N migration to the water table. Processes controlling NO_3^-—N dynamics at locations with near-saturated conditions, showed more complexity: a combination of dilution, transport and reactions such as nitrification/denitrification took placed. As vegetation growth was impeded, microorganisms enhanced production (nitrification) at the soil surface, and possibly denitrification at deeper layers.

In spite of insufficient data, HYDRUS-1D was an effective simulation tool for assessing fate and transport of some N-species. Model simulation results inherit uncertainties produced by several sources (field measurements, modeling approach, model structure and model inputs). Nevertheless, the selected SP-MIM approach produced model results that complemented field data interpretation adequately well. Statistical measures of model goodness of fit (ME, MAE and RSME) were within values commonly reported in the literature for similar processes. Model sensitivity was tested for two transport related parameters, K_d and concentration of ammonium of incoming water (C_{TOP}). Modeled values were not sensitive to K_d but showed incipient sensitivity to C_{TOP}. However, the sensitivity coefficient remained always less than one, denoting model robustness.

Previous knowledge from modeling work conducted at the site using the MIM approach for Cl^- has facilitated the exploration of observed NO_3^-—N data, the interpretation of modeling results leading to processes identification, and the need for future research activities. Similar work is encouraged elsewhere to test model capabilities and performance for prediction of the likelihood of NO_3^-—N mobilization from FL operations, extending the analysis to two-dimensional representations and additional chemical species to close the N cycle in these environments.

Acknowledgments

The authors would like to thank the staff of “Los Niños” feedlot establishment for allowing the development of this research, and the Ministerio de Ciencia e Innovación Productiva (MINCyT) (PFIP 2008-1. 2011/2012), Universidad Nacional del Litoral (UNL) (C.A.I.+D 2011, 50120110100261), and Consejo Nacional de Investigaciones Científicas y Técnicas (CONICET) (Postdoctoral Fellowship No. 161539) for their partial financial support. The authors are also grateful to the anonymous reviewer whose comments and suggestions helped to enhance the quality of this work.

References

Allen, R.G., Pereira, L.S., Raes, D., Smith, M., 1998. Crop Evapotranspiration – Guidelines for Computing Crop Water Requirements. Irrig. Drain. Pap.FAO, Rome, Italy 56.

Arelovich, H.M., Bravo, R.D., Martínez, M.F., 2011. Development, characteristics, and trends for beef cattle production in Argentina. Animal Frontiers. 1 (2), 37–45.

Baram, S., Arnon, S., Ronen, Z., Kurtzman, D., Dahan, O., 2012a. Infiltration mechanism controls nitrification and denitrification processes under dairy waste lagoon. J. Environ. Qual. 41 (5), 1623–1632.

Baram, S., Kurtzman, D., Dahan, O., 2012b. Water percolation through a clayey vadose zone. J. Hydrol. 424, 165–171.

Berlin, M., Kumar, G.S., Nambi, I.M., 2013. Numerical modeling of the effects of immobile water content on nitrate transport in an unsaturated porous system. Cii International Journal of Data Mining Knowledge Engineeering (DOI: DMKE042013004).

Chevron, B., Coquet, Y., 2008. Sensitivity analysis of transient-MIM HYDRUS-1D: Case study Related to pesticide fate in soils. Vadose Zone J. 8 (4), 1064–1079.

Clesceri, L.S., Greenberg, A.E., Eaton, A.E., 1998. Standard Methods for the Examination of Water and Wastewater. American Public Health Association. (ed. 20). Washington, DC.

Crevoisier, D., Popova, Z., Mailhol, J.C., Ruelle, P., 2008. Assessment and simulation of water and nitrogen transfer under furrow irrigation. Agric. Water Manag. 95 (4), 354–366.

Czapar, G.F., Kanwar, R.S., Fawcett, R.S., 1994. Herbicide and tracer movement to field drainage tiles under simulated rainfall conditions. Soil Tillage Res. 30, 1932.

Derby, N.E., Knighton, R.E., 2001. Field-scale preferential transport of water and chloride tracer by depression-focused recharge. J. Environ. Qual. 30, 194–199.

Elliott, L.F., McCalla, T.M., Mielke, L.N., Travis, T.A., 1972. Ammonium, nitrate, and total nitrogen in the soil water of feedlot and field soil profiles. Appl. Microbiol. 23 (4), 810–813.

Feddes, R.A., Bresler, E., Neuman, S.P., 1974. Field test of a modified numerical model for water uptake by root systems. Water Resour. Res. 10 (6), 1199–1206.

Flury, M., Flühler, H., Jury, W.A., Leuenberger, J., 1994. Susceptibility of soils to preferential flow of water: a field study. Water Resour. Res. 30 (7), 1945–1954.

García, A.R., Maisonnave, R., Massobrio, M.J., de Iorio, F., Alicia, R., 2012. Fieldscale evaluation of water fluxes and manure solution leaching in feedlot pen soils. J. Environ. Qual. 41 (5), 1591–1599.

Gee, G.W., Bauder, J.W., Klute, A., 1986. Particle-size analysis. Methods of soil analysis. Part 1. Physical and Mineralogical Methods, pp. 383–411.

Gerke, H.H., van Genuchten, M.T., 1993. A dual-porosity model for simulating the preferential movement of water and solutes in structured porous media. Water Resour. Res. 29, 305–319.

Glaesner, N., Gerke, H.H., 2013. Single and double porosity modeling of solute transport in intact soil columns – effects of texture, slurry placement, and intermittent irrigation. HYDRUS Conference/Workshop, March 2013. Czech Republic, Prague.

Greve, A., Andersen, M.S., Acworth, R.I., 2010. Investigations of soil cracking and preferential flow in a weighing lysimeter filled with cracking clay soil. J. Hydrol. 393 (1), 105–113.

Guevara, J.C., Grünwaldt, E.G., 2012. Status of Beef Cattle Production in Argentina Over the Last Decade and Its Prospects, Livestock Production, Dr. Khalid Javed (Ed.), ISBN: 978-953-51-0814-6, InTech, DOI: http://dx.doi.org/10.5772/50971. (Available from: http://www.intechopen.com/books/livestock-production/status-of-beef-cattle-production-in-argentina-over-the-last-decade-and-its-prospects. Last accessed: May 08, 2016).

Hanson, B.R., Simůnek, J., Hopmans, J.W., 2006. Evaluation of urea–ammonium–nitrate fertigation with drip irrigation using numerical modeling. Agric.Water Manag. 86 (1), 102–113.

Hill, M., 1998. Methods and guidelines for effective model calibration. U.S. Geological Survey. Water-resources Investigations Report 98-4005 (90 pp).

Imhoff, S., Ghiberto, P.J., Grioni, A., Gay, J.P., 2010. Porosity characterization of Argiudolls under different management systems in the Argentine Flat Pampa. Geoderma 158 (3), 268–274.

INTA, 1992. Soil Maps of Argentine Republic, Sheet 3160–14-San Justo.

Jarvis, N.J., 2007. A review of non-equilibrium water flow and solute transport in soil macropores: principles, controlling factors and consequences for water quality. Eur. J. Soil Sci. 58, 523–546.

Johnsson, H., Bergström, L., Jansson, P.-E., Paustian, K., 1987. Simulated nitrogen dynamics and losses in a layered agricultural soil. Agric. Ecosyst. Environ 18, 333–356.

Kachanoski, R.G., Rudra, R., Pringle, E.A., 1992. Technology evaluation and development sub-program; final report: effects of on quality and quantity of surface and subsurface drainage water: Uplands. Ontario Ministry of Agriculture. Guelph, ON, Food and Rural Affairs.

Köhne, J.M., Köhne, S., Simůnek, J., 2009. A review of model applications for structured soils: a) water flow and tracer transport. J. Contam. Hydrol. 104 (1), 4–35.

Kremen, A., Bear, J., Shavit, U., Shaviv, A., 2005. Model demonstrating the potential for coupled nitrification denitrification in soil aggregates. Environ. Sci. Technol. 39 (11), 4180–4188.

Lee, M.S., Lee, K.K., Hyun, Y., Clement, T.P., Hamilton, D., 2006. Nitrogen transformation and transport modeling in groundwater aquifers. Ecol. Model. 192 (1), 143–159.

Lobb, D.A., Kachanoski, R.G., Miller, M.H., 1999. Tillage translocation and tillage erosion in the complex upland landscapes of southwestern Ontario. Canada. Soil Tillage Res. 51, 189–209.

Mailhol, J.C., Crevoisier, D., Triki, K., 2007. Impact of water application conditions on nitrogen leaching under furrow irrigation: experimental and modelling approaches. Agric. Water Manag. 87, 275–284.

Mantovi, P., Fumagalli, L., Beretta, G.P., Guermandi, M., 2006. Nitrate leaching through the unsaturated zone following pig slurry applications. J. Hydrol. 316 (1), 195–212.

Maule, C.T., Fonstad, T.A., 2000. Impacts of cattle penning on groundwater quality beneath feedlots. Can. Agric. Eng. 42 (2), 87–93.

Maule, C.T., Fonstad, T.A., 2002. Solute and moisture flux beneath cattle feedlot pens. Transactions of the ASAE 45 (1), 73–81.

Mielke, L.N., Mazurak, A.P., 1976. Infiltration of water on a cattle feedlot. Transactions of the ASAE 19 (2), 341–0344.

Mielke, L.N., Swanson, N.P., McCalla, T.M., 1974. Soil profile conditions of cattle feedlots. J. Environ. Qual. 3 (1), 14–17.

Miller, J.J., Curtis, T., Larney, F.J., McAllister, T.A., Olson, B.M., 2008. Physical and chemical properties of feedlot pen surfaces located on moderately coarse–and moderately fine–textured soils in Southern Alberta. J. Environ. Qual. 37 (4), 1589–1598.

Olson, B.M., Miller, J.J., Rodvang, S.J., Yanke, L.J., 2005. Soil and groundwater quality under a cattle feedlot in southern Alberta. Water Qual. Res. J. Can. 40 (2), 131–144.

Pepple, L.M., Andersen, D.S., Burns, R.T., Moody, L.B., 2011. Physical and chemical properties of runoff effluent from beef feedlots in Iowa. Trans. ASABE 54 (3), 1079–1084.

Pordomingo, A.J., 2003. Gestión ambiental en el feedlot. Guía de buenas prácticas. INTA Anguil 90.

Prosser, J.I., 1989. Autotrophic nitrification in bacteria. Adv. Microb. Physiol. 30, 125–181.

Ramos, T.B., Šimůnek, J., Gonçalves, M.C., Martins, J.C., Prazeres, A., Castanheira, N.L., Pereira, L.S., 2011. Field evaluation of a multicomponent solute transport model in soils irrigated with saline waters. J. Hydrol. 407 (1), 129–144.

Ramos, T.B., Šimůnek, J., Gonçalves, M.C., Martins, J.C., Prazeres, A., Pereira, L.S., 2012. Two-dimensional modeling of water and nitrogen fate from sweet sorghum irrigated with fresh and blended saline waters. Agric. Water Manag. 111, 87–104.

Richards, L.A., 1931. Capillary conduction of liquids through porous mediums. J. Appl. Phys. 1 (5), 318–333.
Rodríguez, L., Cello, P., Vionnet, C., Goodrich, D., 2008. A fully conservative coupling of HEC-RAS with MODFLOW to simulate stream-aquifer interactions in a drainage system. J. Hydrol. 353, 129–142.
Santini, A., Romano, N., Ciollaro, G., Comegna, V., 1995. Evaluation of a laboratory inverse method for determining unsaturated hydraulic propierties of a soil under different tillage practices. Soil Sci. 160 (5), 340–351.
Saso, J.K., Parkin, G.W., Drury, C.F., Lauzon, J.D., Reynolds, W.D., 2012. Chloride leaching in two Ontario soils: Measurement and prediction using HYDRUS-1D. Can. J. Soil Sci. 92 (2), 285–296.
Schaap, M.G., Leij, F.J., 1998a. Database-related accuracy and uncertainty of pedotransfer functions. Soil Sci. 163 (10), 765–779.
Schaap, M.G., Leij, F.J., 1998b. Using neural networks to predict soil water retention and soil hydraulic conductivity. Soil Tillage Res. 47 (1), 37–42.
Schaap, M.G., Leij, F.J., van Genuchten, M.T., 2001. ROSETTA: a computer program for estimating soil hydraulic parameters with hierarchical pedotransfer functions. J. Hydrol. 251 (3), 163–176.
Schuh, W.M., Klinkebiel, D.L., Gardner, J.C., Meyer, R.F., 1997. Tracer and nitrate movement to groundwater in the Northern Great Plains. J. Environ. Qual. 26, 1335–1347.
Šimůnek, J., van Genuchten, M.T., Šejna, M., 2005. The HYDRUS-1D software package for simulating the one-dimensional movement of water, heat, and multiple solutes in variably-saturated media. Version 3.0, HYDRUS Software Series 1. Department of Environmental Sciences, University of California Riverside, Riverside, CA 270 pp.
Šimůnek, J., van Genuchten, M.T., Šejna, M., 2006. The HYDRUS software package for simulating two- and three-dimensional movement of water, heat, and multiple solutes in variably-saturated media. Technical Manual. Version 1.0. PC Progress, Prague, Czeck Republic 241 pp.
Šimůnek, J., van Genuchten, M.T., Šejna, M., 2008. Development and applications of the HYDRUS and STANMOD software packages and related codes. Vadose Zone J. 7 (2), 587–600.
Šimůnek, J., van Genuchten, M.T., Šejna, M., 2016. Recent developments and applications of the HYDRUS Computer Software Packages. Vadose Zone J. http://dx.doi.org/10.2136/vzj2016.04.0033.
Smith, M.S., Tiedje, J.M., 1979. Phases of denitrification following oxygen depletion in soil. Soil Biol. Biochem. 11 (3), 261–267.
Sweeten, J.M., 2000. Manure and wastewater management for cattle feedlots. Reviews of Environmental Contamination and Toxicology. Springer, New York, pp. 121–153.
Tyler, D.D., Thomas, G.W., 1977. Lysimeter measurements of nitrate and chloride losses from soil under conventional and no tillage corn. J. Environ. Qual. 6, 63–66.
Vaillant, G.C., Pierzynski, G.M., Ham, J.M., DeRouchey, J., 2009. Nutrient accumulation below cattle feedlot pens in Kansas. J. Environ. Qual. 38 (3), 909–918.
Van Dam, J.C., Hendrickx, J.M.H., Van Ommen, H.C., Bannink, M.H., Van Genuchten, M.T., Dekker, L.W., 1990. Water and solute movement in a coarse-textured water-repellent field soil. J. Hydrol. 120 (1–4), 359–379.
van Genuchten, M.T., 1980. A closed-form equation for predicting the hydraulic conductivity of unsaturated soils. Soil Sci. Soc. Am. J. 44 (5), 892–898.
van Genuchten, M.T., Nielsen, D., 1985. On describing and predicting the hydraulic properties of unsaturated soils, Ann. Geophysics 3 (5), 615–628.
van Genuchten, M.T., Wierenga, P.J., 1976. Mass transfer studies in sorbing porous media I. Analytical solutions. Soil Sci. Soc. Am. J. 40 (4), 473–480.
Veizaga, E.A., 2015. Study of the dynamics of nitrate in soil coming from intensive livestock farming (In Spanish) (Doctoral thesis) Universidad Nacional del Litoral, Santa Fe, Argentina http://dx.doi.org/10.13140/RG.2.1.5064.3685.
Veizaga, E.A., Rodríguez, L.B., Ocampo, C.J., 2015. Water and chloride transport in a fine-textured soil in a feedlot pen. J. Contam. Hydrol. 182, 91–103.
Ventrella, D., Mohanty, B.P., Simůnek, J., Losavio, N., van Genuchten, M.T., 2000. Water and chloride transport in a fine-textured soil: field experiments and modeling. Soil Sci. 165 (8), 624–631.
Weihermüller, L., Kasteel, R., Vanderborght, J., Pütz, T., Vereecken, H., 2005. Soil water extracti on with a sucti on cup: results of numerical simulati ons. Vadose Zone J. 4, 899–907.
Weihermüller, L., Kasteel, R., Vanderborght, J., Šimůnek, J., Vereecken, H., 2011. Uncertainty in pesticide monitoring using suction cups: evidence from numerical simulations. Vadose Zone J. 10 (4), 1287–1298.
Wyngaard, N., Videla, C., Picone, L., Zamuner, E., Maceira, N., 2012. Nitrogen dynamics in a feedlot soil. J. Soil Sci. Plant Nutr. 12 (3), 563–574.
Zheng, C., Bennett, G.D., 2002. Applied Contaminant Transport Modeling. vol. 2. Wiley-Interscience, New York.